Tracking the Dynamics of Air Pollution in Northern Thailand: A Spatio-Temporal Analysis Using Ground Sensor Data and NASA's DC-8 Aircraft Observations

Samphutthanont, R.,[1,2*] Mahavik, N.[3,4] and Suwan, M.[2,5]
[1]Department of Geography and Geoinformatics, Faculty of Humanities and Social Sciences
Chiang Mai Rajabhat University, Thailand, E-mail: ratchaphon_sam@cmru.ac.th*
[2]Asian Air Quality Operations Center by Space Technology, Geoinformatics and Environmental Engineering (AiroTEC), Chiang Mai Rajabhat University, Thailand
[3]Department of Natural Resources and Environment, Faculty of Agriculture Natural Resources and Environment, Naresuan University, Thailand, E-mail: nattaponm@nu.ac.th
[4]Water Resources Research Center, Faculty of Engineering, Naresuan University, Thailand
[5]Graduate School, Chiang Mai Rajabhat University, Thailand, E-mail: manatsuwan@gmail.com
ORCID ID: https://orcid.org/0009-0003-7804-5356
**Corresponding Author*

DOI: https://doi.org/10.52939/ijg.v21i10.4523

Abstract
The vertical structure and transboundary transport mechanisms of severe seasonal air pollution in Northern Thailand remain poorly understood, despite posing significant health and environmental challenges. This research examines the spatio-temporal dynamics of air pollution in Northern Thailand, with a particular focus on the Chiang Mai–Lamphun basin. This study integrates data from ground-based IoT sensors, airborne measurements by NASA's Douglas DC-8 research aircraft, satellite-detected fire hotspots, radiosonde meteorological soundings, and the HYSPLIT trajectory model. Results indicate that $PM_{2.5}$ concentrations typically peak in the morning and decline in the afternoon, in association with atmospheric stagnation and temperature inversions. Spatial analysis reveals distinct patterns of pollutant distribution correlated with hotspot locations and wind trajectories transporting emissions from transboundary biomass burning sources. Vertical profile data from the DC-8 aircraft indicate substantial pollutant accumulation in the lower troposphere (1,500 – 3,000 meters above ground level), situated just above the Planetary Boundary Layer (PBL), beneath multiple inversion layers and weak upper-level winds. These conditions facilitate the formation of recirculation zones and enhance pollutant trapping. Skew-T Log-P diagrams further confirm pronounced atmospheric stratification and low CAPE values, indicating limited vertical air exchange. This study emphasizes the critical role of incorporating vertical atmospheric profiles into air quality forecasting systems, especially in basin topographies prone to pollution accumulation. The findings inform the development of proactive early warning systems, designated pollution control zones, and more effective emission control strategies particularly along prevailing wind corridors. Accordingly, continuous monitoring of both horizontal and vertical pollution patterns, along with integration of transboundary pollution data, is thus recommended to enhance sustainable air pollution quality management.

Keywords: Air Pollution, Ground Sensor, NASA DC-8, Spatio-Temporal Analysis, Temperature Inversion

1. Introduction

Over the past decade, air pollution has increasingly been recognized as a critical global environmental challenge, exerting profound adverse effects on human health and quality of life. Among various types, ambient air pollution has garnered considerable attention worldwide. The World Health Organization [1] reported that over 99% of the global population resides in regions where pollutant concentrations exceed recommended guidelines. Such exposure has been linked to elevated risks of cardiovascular diseases, stroke, chronic respiratory conditions, lung cancer, and acute respiratory infections [2]. Furthermore, the State of Global Air 2024 report indicated that air pollution was responsible for more than 8.1 million premature deaths worldwide in 2021.

On average, global life expectancy was reduced by one year and eight months due to air pollution exposure particularly in low- and middle-income countries that rely on biomass fuels and lack effective pollution control measures [3] and [4].

In Thailand, the northern region especially Chiang Mai province has experienced severe air pollution, characterized by notably high concentrations of fine particulate matter ($PM_{2.5}$) during the dry season. These elevated levels are primarily attributed to both local and transboundary biomass burning [5] and [6]. Previous studies have documented a clear deterioration in air quality throughout Northern Thailand, where elevated levels of $PM_{2.5}$, PM_{10}, NO_2, and O_3 are significantly linked to increased public health risks, including cardiovascular diseases, lung cancer, and chronic respiratory diseases such as chronic obstructive pulmonary disease (COPD) [7][8] and [9]. The health burden attributed to $PM_{2.5}$ exposure encompasses considerable losses in years of life, rising mortality rates, and increased hospital admissions for ailments such as skin conditions, conjunctivitis, and stroke, particularly in vulnerable areas like Chiang Mai [10].

Geographical and meteorological factors in the Chiang Mai–Lamphun basin play a critical role in the accumulation of air pollution. The basin is topographically enclosed by high mountain ranges, which restrict vertical air dispersion, particularly during the dry season from March to May. This period is characterized by high temperatures, stagnant winds, and frequent temperature inversion events, all of which facilitate the accumulation of fine particulate matter such as $PM_{2.5}$ [11][12] and [13]. Long-term monitoring has demonstrated that $PM_{2.5}$ concentrations frequently exceed both national and international air quality standards, particularly in March [14]. Consequently, Chiang Mai has consistently been ranked among the cities with the poorest air quality worldwide during March over multiple consecutive years [15].

The principal sources of pollution within the study area are open biomass burning (OBB), which encompasses the combustion of agricultural residues and wildfires. These processes emit fine particulate matter ($PM_{2.5}$) alongside organic compounds, including levoglucosan and acetonitrile, which function as chemical markers indicative of biomass combustion [16] and [17]. Several studies in Europe and Asia have found that levoglucosan is associated with biomass burning activities, particularly during the winter season. [18] and [19]. Similarly, emissions from urban traffic, such as NO_2 and O_3, play a significant role in the formation of secondary pollution through photochemical processes [20] and [21].

Despite extensive analyses of $PM_{2.5}$ and PM_{10} concentration levels in Northern Thailand, the majority have been confined to statistical evaluations of daily or monthly average data. These studies often lack comprehensive integration of spatial and temporal dynamics across both horizontal and vertical dimensions [12] and [22]. Furthermore, the ground-based monitoring network exhibits limitations in spatial coverage within the Chiang Mai–Lamphun basin, and most research also lacks measurements from the lower troposphere, which are crucial for understanding the mechanisms of pollutant accumulation at various altitudes. The vertical data constraints hinder comprehensive tracking of pollutant behavior under complex conditions, especially during temperature inversions and atmospheric stagnation [23] and [24].

To address this knowledge gap, the study employs Geographic Information Systems (GIS) to perform a comprehensive analysis of air pollution dynamics. This investigation integrates data from multiple sources, including air quality monitoring stations operated by the Pollution Control Department (PCD), IoT-based $PM_{2.5}$ sensors providing detailed localized measurements within the study area, airborne data collected by NASA's Douglas DC-8 aircraft as part of the ASIA-AQ (Airborne and Satellite Investigation of Asian Air Quality) project [25], satellite-derived emission source information, and meteorological observations obtained from radiosonde balloon measurements. These datasets are combined with wind field data and trajectory modeling to explore the influence of meteorological conditions on temporal and spatial variations in air pollutant concentrations.

Accordingly, this research aims to: 1. Collect and integrate air pollution data from ground-based sensors and NASA's DC-8 aircraft observations; 2. Analyze the spatio-temporal and vertical dynamics of fine particulate matter; and 3. Investigate the meteorological factors driving pollutant accumulation and dispersion. The findings are expected to enhance understanding of pollutant structure and dynamics within the Chiang Mai–Lamphun basin, thereby supporting the development of improved forecasting models, early warning systems, and spatial planning strategies for future environmental management.

2. Material and Methods

2.1 Study Area

The study area for this research is located in Northern Thailand, specifically defined within the Chiang Mai–Lamphun Basin, which encompasses the principal cities of Chiang Mai and Lamphun. The study site lies between latitudes 18.554824° and 18.906203° N and longitudes 98.895657° and 99.175350° E. The topography of the Chiang Mai–Lamphun Basin is characterized by a bowl-shaped depression surrounded by high mountain ranges. To the west, the Thanon Thong Chai Mountain Range extends longitudinally in a north-south direction, while to the east, the Khun Tan Range runs parallel in a similar north-south orientation. The basin's flatlands range in elevation from approximately 280 to 360 meters above sea level, a factor that significantly influences atmospheric circulation and the retention of pollutants within the atmospheric boundary layer. During the dry season, open biomass burning commonly occurs, resulting in severe accumulation of haze and fine particulate matter, particularly in March each year. The study area within Chiang Mai–Lamphun basin covers approximately 1,000 square kilometers (Figure 1). The black rectangular frame delineates the boundary of the study area. White triangles and squares denote the locations of Chiang Mai and Lamphun cities, respectively. Green flag-shaped markers indicate the positions of the Pollution Control Department's Air Quality Monitoring Stations. Blue triangles represent the installation sites of HAZEMON sensors. The red, purple, yellow, and blue dashed lines correspond to the flight paths of the DC-8 aircraft on March 16, 18, 21, and 25, 2024, respectively.

2.2 Data Sources and Methods

2.2.1 Pollution control department's air quality monitoring station

In this study, hourly averaged $PM_{2.5}$ concentration data from the Pollution Control Department (PCD) air quality monitoring stations were utilized as a reference dataset for comparison and validation against data obtained from HAZEMON sensors. These measurements were collected from three PCD stations located within the study area, specifically in the urban zones of Chiang Mai and Lamphun. The three stations include Station 35T (latitude 18.840732, longitude 98.969780), Station 36T (latitude 18.790933, longitude 98.990000), and Station 68T (latitude 18.567194, longitude 99.038639). Data collection was conducted over the period from 14 to 25 March 2024, corresponding with the timeframe of the ASIA-AQ campaign and the NASA DC-8 research flights. These ground-based observations play a critical role in assessing the accuracy and consistency of the IoT-based ground sensor network in monitoring the dynamics of air pollution within the Chiang Mai–Lamphun Basin.

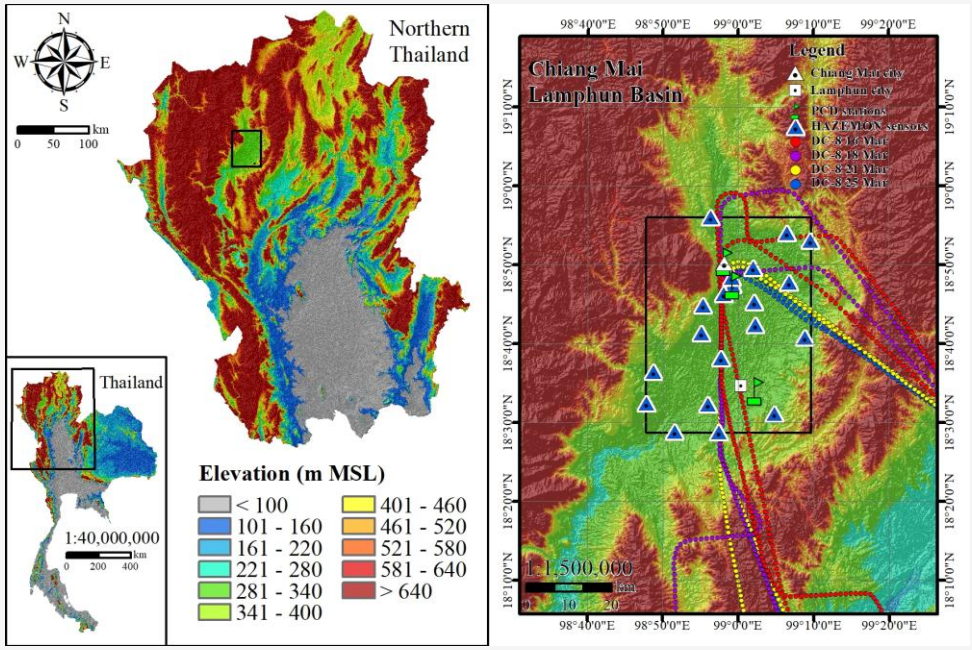

Figure 1: Northern region of Thailand, ground sensor locations, and DC-8 flight paths

2.2.2 HAZEMON sensor

The HAZEMON IoT sensor system employed in this study was developed by the Internet Education and Research Laboratory (intERLab) at the Asian Institute of Technology (AIT) [26][27] and [28] in collaboration with AiroTEC of Chiang Mai Rajabhat University (CMRU). The sensors were deployed throughout the study area to facilitate real-time air quality monitoring. The HAZEMON sensors are designed to detect particulate matter with a diameter of less than 2.5 microns ($PM_{2.5}$), capturing data at one-minute intervals. These raw data were subsequently aggregated into hourly averages for further analysis.

To verify the accuracy and reliability of the data collected by the HAZEMON sensors, a validation process was undertaken by comparing sensor measurements with reference data from three proximate air quality monitoring stations operated by the Pollution Control Department (PCD), namely Stations 35T, 36T, and 68T. The analysis revealed high correlation coefficients of 0.9336, 0.86559, and 0.9280, respectively, between the HAZEMON and PCD datasets. These results demonstrate a strong agreement between the two data sources, confirming the robustness and credibility of the HAZEMON sensor system for monitoring fine particulate matter in the study area and thereby providing field verification that ensures the reliability of the dataset for subsequent spatial and temporal analyses.

Subsequently, a simple linear regression model was developed to calibrate the HAZEMON sensor measurements, ensuring consistency with the reference values provided by the Pollution Control Department (PCD). The regression equation is defined in Equation 1:

$$y = 0.4427x + 20.299 \quad \text{Equation 1}$$

Where:

y = Adjusted $PM_{2.5}$ concentration (µg/m³)

x = $PM_{2.5}$ concentration measured by the HAZEMON sensor (µg/m³)

For data collection in the study area, a total of 20 HAZEMON sensors were deployed across the entire region (Table 1). A 10 × 10 kilometer grid system was utilized to ensure systematic spatial coverage, with sensors strategically installed at suitable locations within each grid cell to enable high-resolution monitoring of $PM_{2.5}$ concentrations. Data were collect during the period from March 14 to 25, 2024, aligning with the ASIA-AQ Thailand campaign and the NASA DC-8 research aircraft missions.

2.2.3 Aircraft observation data

The aircraft-based data utilized in this study were obtained from NASA's DC-8 research aircraft as part of the ASIA-AQ project, a collaborative initiative between NASA and several international research institutions. The primary objective of the project is to investigate the sources, distribution, and transformation of air pollutants in the lower troposphere over Southeast Asia throgh the integration of satellite observations, ground-based measurements, and airborne monitoring. In addition, the mission seeks to assess the impact of emissions from Asia on the chemical composition of the atmosphere over the North Pacific Ocean and underscores the importance of sustained air quality monitoring [29] and [30]. For this study, data were obtained from NASA DC-8 flight campaigns conducted over Thailand on March 16, 18, 21, and 25, 2024 periods that coincided with the peak of the haze pollution crisis in Northern Thailand. The aircraft operated two daily flights over the study area, one in the morning and one in the afternoon. Each flight involved take-off and landing procedures at Chiang Mai International Airport using a "missed approach" pattern, which resulted in varying altitudes and flight times across missions. Detailed flight parameters are summarized in Table 2. Data were recorded every 10 seconds within the study domain, providing high temporal resolution for capturing the dynamic behavior of air pollutants.

Table 1: HAZEMON sensor deployment locations

No	Latitude	Longitude	Elevation (m MSL)	No	Latitude	Longitude	Elevation (m MSL)
1	18.679824	99.148971	312.01	11	18.806094	98.987099	316.32
2	18.791561	98.988088	312.30	12	18.540630	98.797866	331.92
3	18.636152	98.963498	296.40	13	18.479470	98.958626	308.58
4	18.748129	98.923743	340.97	14	18.771393	98.969115	308.27
5	18.705944	99.038873	300.78	15	18.884308	99.161025	364.62
6	18.899974	99.108658	339.67	16	18.827431	99.034726	312.06
7	18.796388	99.113320	309.35	17	18.688729	98.919252	315.18
8	18.519478	99.081652	332.96	18	18.754172	99.037008	300.98
9	18.538466	98.934307	292.01	19	18.933431	98.940445	327.01
10	18.481271	98.860461	285.46	20	18.607627	98.814068	331.76

Table 2: DC-8 flight data over the study area

Flight Date/ Session		Latitude(°N) (Start-End)	Longitude(°E) (Start-End)	Flight Time(hh:mm:ss) (Start-End)	Flight Altitude(m) (Min-Max)
March 16	Morning	18.486710-18.893391	99.022612-99.152613	11:52:35–12:04:05	2,142-2,537
	Afternoon	18.481162-18.803883	98.985976-99.150686	15:49:35-15:59:35	345-3,024
March 18	Morning	18.484813-18.931445	98.962135-98.962260	10:25:05-10:33:25	304-1,701
	Afternoon	18.484567-18.828520	98.963861-99.148963	14:30:55- 14:40:15	350-2,341
March 21	Morning	18.482439-18.740508	98.962512-99.159590	10:01:55-10:11:55	282-2,051
	Afternoon	18.480178-18.734495	98.959747-99.158375	14:15:25-14:25:15	339-2,168
March 25	Morning	18.482168-18.726080	98.963503-99.157929	09:51:35-10:01:35	301-2,165
	Afternoon	18.481384-18.717946	98.962198-99.150036	13:48:55-13:58:45	334-2,175

The dataset includes latitude–longitude coordinates, timestamps, altitude levels (derived from air pressure), and concentrations of major atmospheric pollutants. Specifically, Levoglucosan ($C_6H_{10}O_5$) was measured using the CHARON instrument; Acetonitrile (CH_3CN) by PTR-MS; Ozone (O_3) by ROZE; and Nitrogen Dioxide (NO_2) by FRANCHIN. Levoglucosan and Acetonitrile serve as key tracers for biomass burning events, such as forest fires and agricultural residue combustion, while NO_2 functions as a precursor for the formation of secondary $PM_{2.5}$. Accordingly, the dataset from this airborne campaign is critical for examining pollution sources and understanding the spatio-temporal dynamics of air quality deterioration in the Chiang Mai–Lamphun basin.

2.2.4 Satellite data

This study employed satellite-based data to monitor the sources of air pollution, with a particular focus on identifying fire hotspots associated with open biomass burning one of the primary contributors to fine particulate matter ($PM_{2.5}$) in the region. Hotspot information was derived from the Visible Infrared Imaging Radiometer Suite (VIIRS) sensor onboard the Suomi National Polar-orbiting Partnership (Suomi NPP) satellite. VIIRS utilizes thermal infrared detection technology to capture heat signatures from surface fires, offering a spatial resolution of up to 375 meters. The satellite operates in a sun-synchronous orbit, enabling it to provide global observations twice daily [31] and [32]. Over Northern Thailand, the satellite passes at approximately 13:30 local time during the ascending node and around 01:30 during the descending node, enabling systematic and temporally consistent monitoring of fire-related emissions in the study area.

Hotspot data from VIIRS were obtained via NASA's Fire Information for Resource Management System (FIRMS), a platform designed to support resource management using wildfire data [33]. For this study, hotspot records corresponding to the period of March 16–25, 2024, were selected, encompassing a radius of 300 kilometers centered on the study area. This spatial extent includes Northern Thailand as well as parts of neighboring countries such as Myanmar and the Lao People's Democratic Republic (Lao PDR), to analyze potential cross-border and inter-provincial pollution sources entering the Chiang Mai–Lamphun basin.

Additionally, this study utilized a Digital Elevation Model (DEM) derived from the ALOS (Advanced Land Observing Satellite) program, developed by the Japan Aerospace Exploration Agency (JAXA) [34]. The DEM, offering a spatial resolution of 12.5 meters, served as a foundational base map to analyze topographical characteristics that affect the accumulation and movement of air pollutants within the study area.

2.2.5 Meteorological data

For the meteorological analysis, this study utilized upper-level wind field data at the 925 hPa pressure level, sourced from the Thai Meteorological Department. These maps provide comprehensive information on wind direction and speed across Thailand and adjacent countries, serving as critical inputs for analyzing the regional dynamics of air mass movement and air pollutant transport (Thai Meteorological Department, 2024). Vertical atmospheric data were obtained from upper-air observations conducted by the Northern Meteorological Center in Chiang Mai Province. These observations included radiosonde soundings, which provide detailed atmospheric profiles visualized through Skew-T Log-P diagrams to represent the thermodynamic structure of the atmosphere. The key variables analyzed comprised temperature, dew point, wind speed and direction, and Convective Available Potential Energy (CAPE). Radiosonde data, collected by the Thai Meteorological Department (TMD) and archived by the University of Wyoming (2025) [35], were retrieved for March 16, 18, 21, and 25, 2024, facilitating the examination of vertical atmospheric profiles and the accumulation patterns of air pollutants.

Additionally, the study utilized precipitation data from the PERSIANN-CDR (Precipitation Estimation from Remotely Sensed Information using Artificial Neural Networks – Climate Data Record) model, developed by the University of California, Irvine. This dataset facilitated a detailed analysis of meteorological conditions and enabled assessment of rainfall's role in the removal and reduction of atmospheric pollutants [36] and [37].

2.2.6 Trajectory model by HYSPLIT

To analyze the trajectories of air masses and the dispersion of pollutants, this study employed the HYSPLIT (Hybrid Single-Particle Lagrangian Integrated Trajectory) numerical model developed by the United States National Oceanic and Atmospheric Administration (NOAA) [38]. The model simulated backward trajectories of air masses over the study area, utilizing meteorological data from the Global Forecast System (GFS), which provides global coverage at a spatial resolution of 0.25 degrees, with data available from June 2019 onward. For the model inputs, this study defined the receptor location at the center of the study area, with coordinates 18.7055°N, 98.9796°E. The backward trajectory analysis was performed for the period from March 16 to 25, 2024, to identify potential sources of pollutants affecting the study region. The total backward run time was set to 72 hours, with simulations conducted at three altitude levels: surface level at 10 meters above ground level (AGL), mid-level atmosphere at 500 meters AGL, and upper-level atmosphere at 1,000 meters AGL. The HYSPLIT trajectory analysis enables identification of pollutant source regions and provides insights into pollutant transport patterns from their origins to the receptor site [38] and [39]. For the analysis of particulate matter sources and transport pathways, the HYSPLIT backward trajectory model was employed, which describes the movement of air parcels as defined in Equation 2:

$$P(t+\Delta t) = P(t) + \frac{1}{2}\left[V(P,t) + V(P',t+\Delta t\right]\Delta t$$

Equation 2

Where:

$P(t)$ = The position vector of an air parcel at time t.

Δt = The time step increment, which is negative for backward trajectory calculations.

$V(P,t)$ = The wind velocity vector at position P and time t.

P' = The predicted intermediate position calculated using $P'=P(t)+V(P,t)\Delta t$.

$V(P', t+\Delta t)$ = The wind velocity vector at the predicted position P' and time $t+\Delta t$.

$P(t+\Delta t)$ = The updated position of the air parcel after the time step Δt.

This equation utilizes a second-order numerical integration method specifically, the modified Euler or second-order Runge-Kutta technique to estimate the trajectory paths of air parcels based on interpolated wind field data.

2.2.7 GIS data and analysis

Geographic Information Systems (GIS) played a pivotal role in this study by integrating diverse datasets from multiple sources, including air quality monitoring stations, ground-based air quality sensors, observational data from NASA's DC-8 research aircraft, hotspot data derived from the VIIRS satellite, precipitation data from the PERSIANN satellite, and air mass trajectory information from numerical models (Table 3). All datasets were transformed into a unified spatial data format (Shapefile) to ensure consistency and were systematically organized within a spatial database. This comprehensive geodatabase facilitated detailed spatial analyses and the production of cartographic visualizations. Furthermore, administrative boundaries at the provincial and national levels, locations of significant landmarks, and basemaps were incorporated to verify spatial accuracy and to support a more comprehensive interpretation and presentation of the study's findings.

The spatial data analysis within the GIS framework was carried out through a series of steps. Hourly Hybrid Single-Particle Lagrangian Integrated Trajectory $PM_{2.5}$ measurements were spatially interpolated using the Ordinary Kriging method [40] to create continuous concentration surfaces for each time interval. Subsequently, these surfaces were classified using the Equal Interval Classification technique to distinctly illustrate spatial distribution patterns. Ordinary Kriging, a widely recognized geostatistical interpolation method, offers unbiased estimates for spatially correlated variables such as $PM_{2.5}$ concentrations by accounting for spatial autocorrelation and the spatial relationships among data points [41] and [42]. The estimation of $PM_{2.5}$ concentrations at locations without direct measurements was performed using the Ordinary Kriging technique, as defined in Equation 3 [43]:

$$\hat{Z}(s_0) = \sum_{i=1}^{n} \lambda_i Z(s_i)$$

Equation 3

Where:

$Z(s_i)$ = the measured value at the i^{th} location
λi = an unknown weight for the measured value at the ith location
s_0 = the prediction location
N = the number of measured values

The hotspot data were analyzed for spatial density using the Kernel Density Estimation (KDE) technique [44]. The analysis was conducted with a cell size of 1 × 1 kilometers and the bandwidth radius set to the default value to calculate the density of hotspots per unit area (points per square kilometer). Subsequently, the density values were classified using the Equal Interval Classification method to categorize the levels of air pollution source intensity for each day. The basic equation for spatial distribution analysis of $PM_{2.5}$ using the Kernel Density Estimation (KDE) technique is defined in Equation 4 [44]:

$$Density = \frac{1}{(radius)^2} \sum_{i=1}^{n} \left[\frac{3}{\pi} pop_i \left(1 - \left(\frac{dist_i}{radius} \right)^2 \right)^2 \right], \text{ for } dist_i < radius$$

Equation 4

Where:

i = 1,…,n are the input points. Only include points in the sum if they are within the radius distance of (x,y) location
pop_i = the population field value of point i, which is an optional parameter
$dist_i$ = the distance between point i and the (x,y) location

The KDE analysis facilitates the generation of a continuous density surface of hotspots, capturing their spatial variability across the study area. Air trajectory analysis utilized output from the HYSPLIT Trajectory model, which was converted into Shapefile format for spatial overlay with hotspot data. The analysis involved quantifying the number of hotspot occurrences intersected by air trajectories within each of the eight principal compass directions: north (N), northeast (NE), east (E), southeast (SE), south (S), southwest (SW), west (W), and northwest (NW). This method enabled the examination of air mass movement patterns and facilitated the identification of potential pollution source regions impacting the study area. Rainfall cluster analysis was performed using PERSIANN satellite data, which was overlaid with hotspot density maps and air trajectory data to assess the impact of precipitation on the reduction of hotspot frequency and atmospheric pollution levels.

Overlay analysis within Geographic Information Systems (GIS) involves integrating spatial data from multiple layers to produce new insights into the spatial relationships among geographic phenomena [45]. This approach is essential for identifying areas where air pollution, emission sources, and meteorological conditions intersect, thereby enhancing the understanding necessary for effective environmental assessment and management. Figure 2 presents the methodological framework applied in this study. The workflow begins with multi-platform data sources, including ground-based $PM_{2.5}$ monitoring, aircraft vertical profiles, satellite observations, meteorological datasets, and HYSPLIT trajectory modeling. These datasets were pre-processed through temporal aggregation on an hourly and daily basis, calibration of HAZEMON sensors with reference to PCD data, and coordinate transformation into a unified GIS database. The analysis incorporated temporal trend analysis, source identification using hotspots and wind fields, and vertical profile interpretation from the NASA DC-8 flights. GIS-based approaches such as ordinary kriging evaluated by RMSE validation, kernel density estimation, and overlay analysis were implemented to evaluate spatial distributions. The kernel density estimation was conducted in GIS software, where the bandwidth was automatically determined using Silverman's Rule of Thumb spatial variant to account for dataset characteristics and spatial outliers. The final outputs included spatio-temporal $PM_{2.5}$ maps, vertical cross-sections of pollutants, and visualization of recirculation zones and inversion layer effects.

3. Results and Discussions

3.1 Temporal Dynamics of $PM_{2.5}$ Concentration

Figure 3 presents the hourly $PM_{2.5}$ concentration data from March 14 to 25. On March 16, the $PM_{2.5}$ concentration peaked at 181.1875 µg/m³, followed by a gradual decrease from March 17 to 19. The lowest concentration was recorded on March 20 at 30.3125 µg/m³, primarily due to the influence of a seasonal thunderstorm. Afterward, $PM_{2.5}$ levels steadily increased from March 21 to 25.

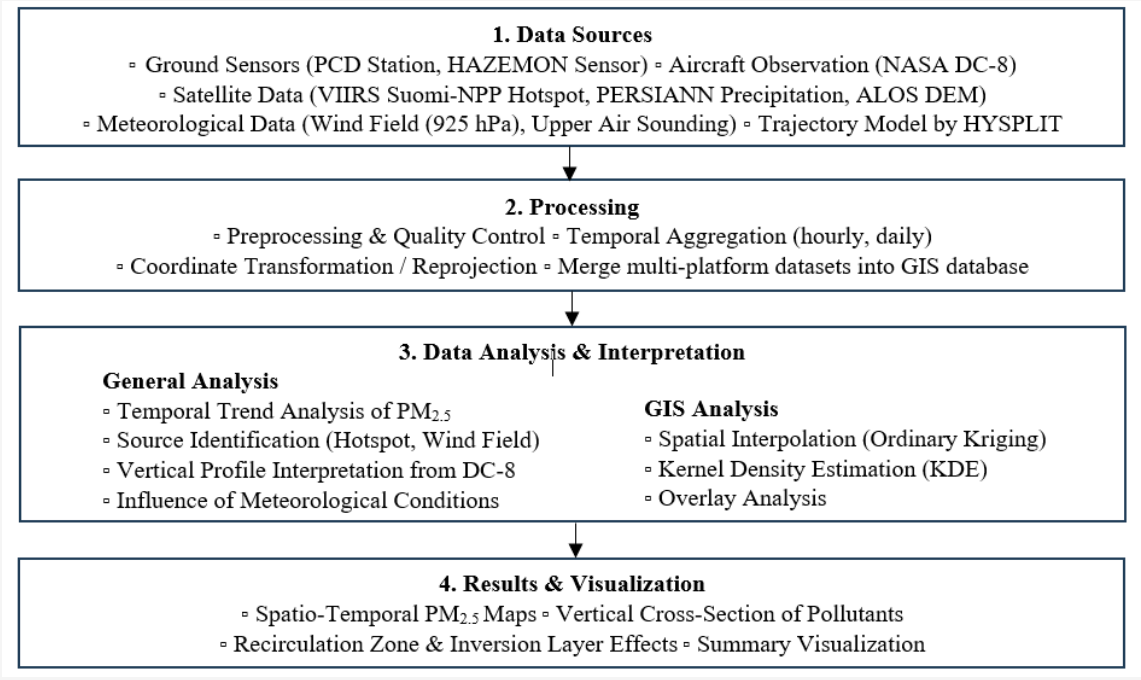

Figure 2: Spatio-temporal dynamics of air pollution study workflow

Table 3: Summary of data sources, resolutions, and key variables used in this study

Data Category	Dataset / Source	Resolution (Spatial / Temporal)	Notes
Ground Sensors	PCD Air Quality Stations (35T, 36T, 68T); Pollution Control Department, Thailand	Point-based / Hourly	Reference $PM_{2.5}$ data for validation and calibration
	HAZEMON IoT Sensors (20 units, AiroTEC CMRU and intERLab AIT)	Point-based (grid 10×10 km) / Hourly	$PM_{2.5}$, regression calibration with PCD
Aircraft Observations	NASA DC-8 (ASIA-AQ Campaign, March 16, 18, 21, 25, 2024)	Flight transects / 10-sec intervals	Levoglucosan (CHARON) Acetonitrile (PTR-MS) Ozone (ROZE) NO_2 (FRANCHIN)
Satellite Data	VIIRS Active Fire / Hotspots (Suomi NPP)	375 m / Twice daily	Biomass burning detection
	PERSIANN-CDR Precipitation (UC Irvine)	0.25° × 0.25° / Daily	Rainfall for pollutant removal assessment
	ALOS DEM (JAXA)	12.5 m / Static	Topography for pollutant accumulation analysis
Meteorological Data	ERA5 Reanalysis Wind Field (925 hPa, European Centre for Medium-Range Weather Forecasts, ECMWF)	0.25° × 0.25° / Hourly	Regional wind dynamics
	Radiosonde Soundings (TMD Chiang Mai, Univ. of Wyoming archive)	Point-based / 1 time daily (morning, 00 UTC)	Vertical profiles: T, RH, wind, CAPE
Trajectory Model	HYSPLIT (NOAA ARL, GFS input)	0.25° / 3-hourly	72-h backward trajectories at 10, 500, 1000 m AGL

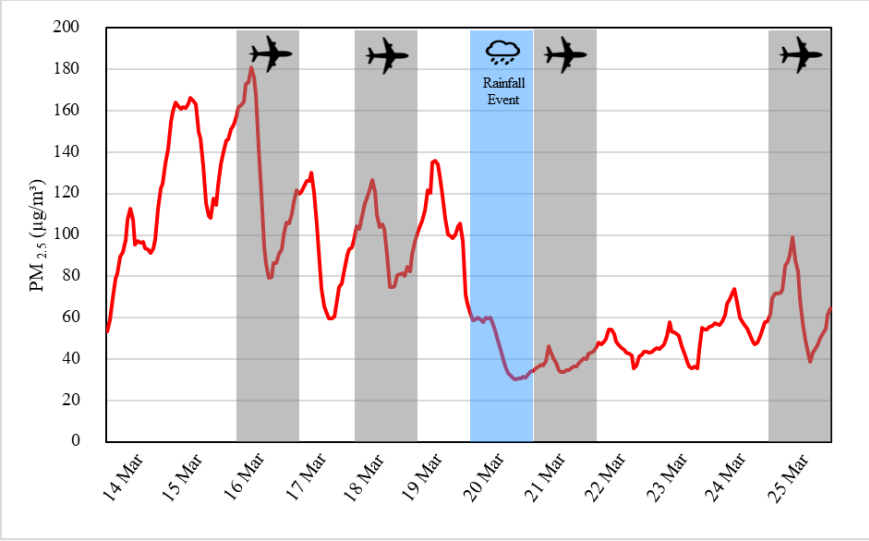

Figure 3: Daily variation of $PM_{2.5}$ concentrations observed at the ground monitoring site from March 14–25, 2024. Gray shading indicates NASA DC-8 flight periods, while the blue shading represents a rainfall event

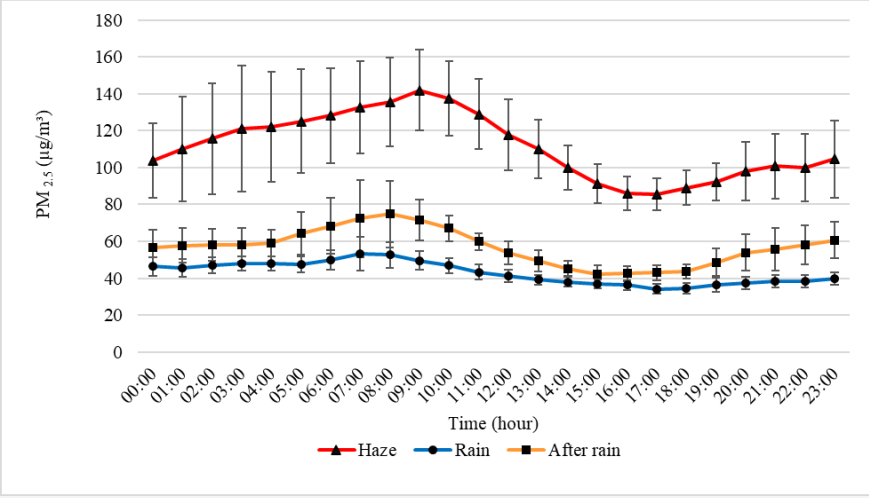

Figure 4: Average hourly variation of $PM_{2.5}$ concentrations under haze, rain, and after-rain conditions. Error bars represent standard deviation of the mean values

Overall, the hourly data exhibited a consistent daily pattern of fluctuations, with concentrations typically peaking in the morning and reaching their lowest values in the evening.

Averaging the $PM_{2.5}$ concentrations from all sensor points between March 14 and 25 on an hourly basis reveals that the highest level during the pollution episode occurred at 9:00 AM, with a concentration of 101.28 µg/m³. The lowest concentration occurred at 5:00 PM, measuring 61.95833 µg/m³. This pattern is closely linked to meteorological conditions: lower temperatures and higher atmospheric pressure tend to trap $PM_{2.5}$ within the basin, especially from early morning until around 9:00 AM. In contrast, as temperatures rise and atmospheric pressure decreases later in the day, pollutants disperse into the upper atmosphere, leading to reduced $PM_{2.5}$ concentrations observedfrom around noon through approximately 5:00 PM.

The analysis divided the study period into three phases: the pollution crisis (March 14–19), the rainy period (March 20–22), and the post-rain period (March 23–25). Distinct temporal patterns of $PM_{2.5}$ concentrations were observed across these phases. The peak concentrations occurred at 9:00 AM during the pollution crisis, 7:00 AM in the rainy period, and 8:00 AM following the rain. Conversely, the lowest concentrations were recorded at 5:00 PM for both the pollution crisis and rainy periods, and at 3:00 PM during the post-rain phase (see Figure 4).

3.2 Spatial Dynamics of $PM_{2.5}$ Distribution Pattern

Spatial interpolation of $PM_{2.5}$ data from all sensor locations revealed a general pattern of elevated concentrations in the morning, followed by a gradual decline from the afternoon into the evening (Figure 5). This trend aligns with findings by [46], who explained that air pollutants such as PM_{10} tend to peak during morning hours due to high emission rates and limited atmospheric dispersion under stable atmospheric boundary layer (ABL) conditions. In contrast, certain regions such as the southern Sahel and the Indian subcontinent have reported elevated nighttime Dust Optical Depth (DOD), attributed to atmospheric dynamics that promote dust mixing and dispersion during the daytime [47].

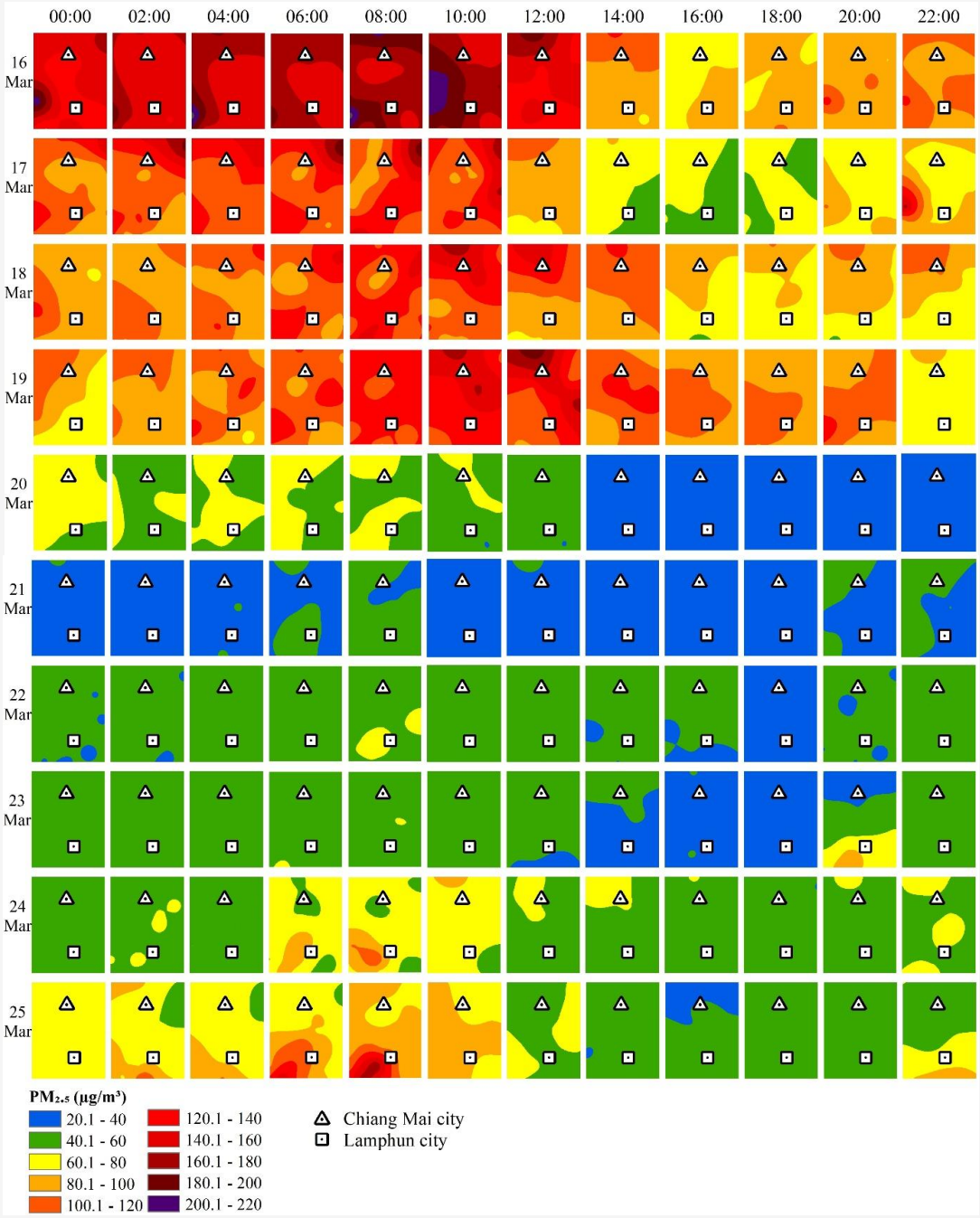

Figure 5: Spatial distribution patterns of PM2.5 concentration at two-hour intervals from March 16 to 25, 2024

Table 4: Root mean square error (RMSE, µg/m3) values from the ordinary kriging interpolation of PM2.5 concentrations

Date/Time	00:00	02:00	04:00	06:00	08:00	10:00	12:00	14:00	16:00	18:00	20:00	22:00	AVG
16 Mar	0.15	35.19	33.30	35.86	7.86	0.10	0.17	0.06	5.96	1.78	0.11	0.13	10.05
17 Mar	0.19	0.16	21.57	0.21	0.20	0.20	0.09	0.06	2.21	0.04	18.03	0.17	3.59
18 Mar	17.86	13.14	0.12	4.54	0.19	0.14	0.16	0.09	3.02	4.89	0.07	0.81	3.75
19 Mar	5.52	26.51	4.35	12.40	2.96	2.06	0.20	0.11	9.56	7.72	7.89	18.68	8.16
20 Mar	9.82	12.14	6.68	2.18	14.18	0.04	6.70	0.02	1.29	0.02	0.77	1.39	4.60
21 Mar	1.38	4.21	0.03	4.34	5.06	5.08	0.03	2.86	2.68	3.50	2.13	3.46	2.90
22 Mar	0.07	0.03	1.55	5.15	0.07	0.11	5.48	1.99	0.02	6.44	1.64	0.06	1.88
23 Mar	8.07	0.86	2.82	10.04	0.58	3.78	0.05	0.03	1.74	2.99	0.09	1.02	2.67
24 Mar	15.68	15.07	6.78	0.10	0.16	7.29	0.02	0.05	0.05	0.04	8.38	1.66	4.61
25 Mar	41.41	0.13	0.11	0.13	0.19	4.17	0.77	2.87	1.75	3.81	4.75	0.10	5.02
AVG	10.01	10.74	7.73	7.49	3.15	2.30	1.37	0.81	2.83	3.12	4.39	2.75	**4.72**

When examining the spatial variation of $PM_{2.5}$ concentrations, it was observed that high-concentration dust clusters typically appeared on one side of the study area. On March 16, the highest concentrations were predominantly located in the western part of the area, whereas on March 17, 18, and 19, the clusters shifted to the northern region. From March 20 to 23, the distribution pattern became more scattered and less defined, likely due to the influence of rainfall, which significantly reduced the concentration of airborne particles. These findings are consistent with studies by [48] and [49]. On March 24 and 25, high-concentration $PM_{2.5}$ clusters reappeared prominently in the southern part of the Chiang Mai–Lamphun Basin (as illustrated in Figure 5). When examined alongside hotspot data representing potential sources of biomass burning a strong correlation was observed. Elevated $PM_{2.5}$ levels consistently coincided with a higher number of hotspots on the same days. This association was further influenced by prevailing wind directions, suggesting that both emission intensity and atmospheric transport played significant roles in the observed pollution patterns.

The spatial distribution patterns of $PM_{2.5}$ in Figure 5 were generated as 1 km raster surfaces using ordinary kriging from 20 HAZEMON sensors and retained in raster format. Comparison with VIIRS hotspot data revealed strong spatial and temporal consistency, indicating that both local emissions and transboundary biomass burning contributed to the observed pollution, as further examined in Section 3.3 through HYSPLIT backward trajectories. The accuracy of the interpolation was evaluated using the ordinary kriging method with cross-validation, where observed values were sequentially excluded and predicted from surrounding data points. The Root Mean Square Error (RMSE) values (Table 4) were then calculated to quantify the differences between observed and predicted $PM_{2.5}$ concentrations. The results show an average RMSE of 4.72, which is considered low and acceptable in terms of prediction accuracy. This indicates that ordinary kriging provides reliable performance in capturing the spatial distribution of $PM_{2.5}$, although localized uncertainty remains in areas with complex variability or sparse monitoring coverage.

3.3 Identification of Air Pollution Sources Using Hotspot Data and Trajectory HYSPLIT Model

Figure 6(a)–(j) illustrates the daily distribution of hotspot locations within a 300-kilometer radius from the center of the study area. As shown in Figure , daily $PM_{2.5}$ concentrations were generally correlated with the number of daily hotspots. This relationship suggests that an increase in hotspot counts is typically associated with higher concentrations of air pollutants such as $PM_{2.5}$, consistent with the findings of [50], who reported a strong correlation between hotspot frequency and the Air Pollution Standard Index. Furthermore, when analyzed alongside the results of the HYSPLIT backward trajectory model, there was a significant spatial and directional consistency, reinforcing the connection between emission sources and pollutant transport pathways. Similarly, in Kalimantan, Indonesia, the HYSPLIT model has been employed to trace PM_{10} emissions from peat fires, demonstrating that wind direction and topography play a significant role in influencing the dispersion of air pollutants [51]. In Chengdu, China, HYSPLIT was instrumental in identifying that the majority of $PM_{2.5}$ and PM_{10} pollution originated from local and regional sources, with some contributions from distant regions such as India and Myanmar underscoring the model's capacity for tracking long-range pollutant transport [52].

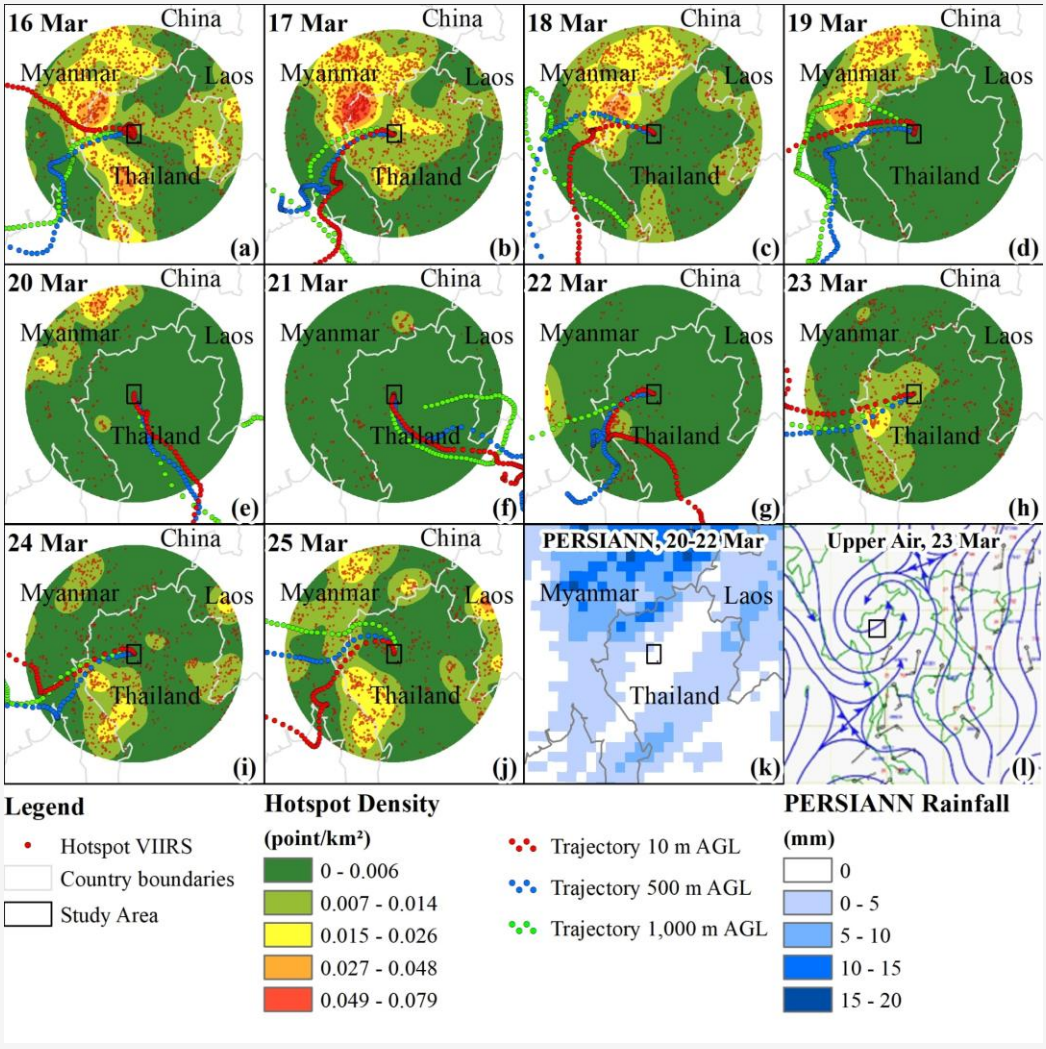

Figure 6: Daily distribution of VIIRS hotspots and 72-h backward trajectories at 10 m AGL, 500 m AGL, and 1,000 m AGL levels during 16-25 March, 2024 (a)–(j). Panel (k) shows accumulated PERSIANN rainfall (20–22 March), and panel (l) illustrates upper-level wind patterns on 23 March, 2024

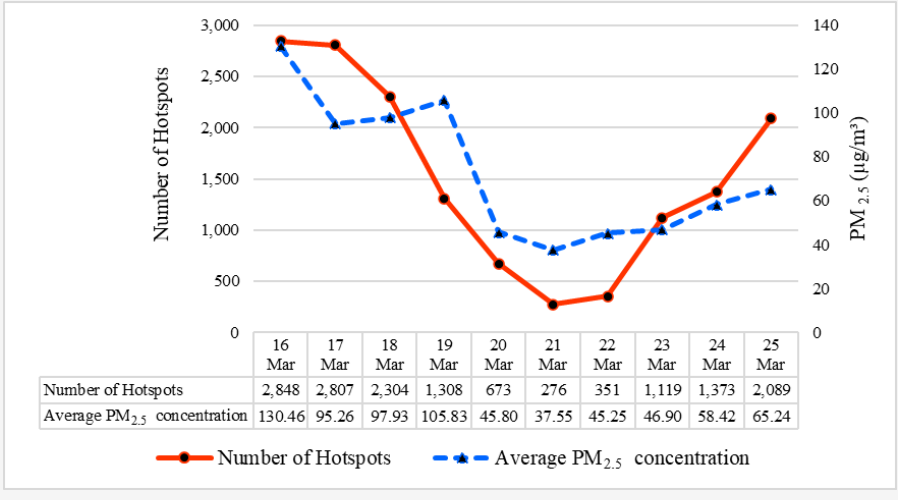

	16 Mar	17 Mar	18 Mar	19 Mar	20 Mar	21 Mar	22 Mar	23 Mar	24 Mar	25 Mar
Number of Hotspots	2,848	2,807	2,304	1,308	673	276	351	1,119	1,373	2,089
Average $PM_{2.5}$ concentration	130.46	95.26	97.93	105.83	45.80	37.55	45.25	46.90	58.42	65.24

Figure 7: Daily number of hotspots and the average $PM_{2.5}$ concentrations from March 16–25, 2024

The model's effectiveness was also demonstrated in Beijing, where it identified regional pollution sources and the major impact of imported pollution from southern cities [53].

High-density hotspot clusters were frequently observed along the air trajectory paths, contributing to elevated PM concentrations. During the critical haze period from March 16 to 19, high-intensity $PM_{2.5}$ clusters were predominantly located in the western and northwestern zones of the study area, covering the Thai border in Mae Hong Son Province and adjacent regions in Myanmar. These areas also exhibited a high number of hotspots, accounting for a substantial proportion of the total daily hotspots: 945 points (33%) on March 16, 1,332 points (47%) on March 17, 916 points (40%) on March 18, and 750 points (57%) on March 19. The Backward Trajectory analysis confirmed that air masses during this period passed through these western regions, indicating a strong link between transboundary pollution sources and increased $PM_{2.5}$ levels.

Between March 20 and 22, increased rainfall and high humidity significantly contributed to a sharp reduction in daily hotspot counts, which dropped to 673, 276, and 351, respectively. During this period, the HYSPLIT Backward Trajectory analysis showed a shift in wind direction, with air masses originating from the south and bypassing major hotspot areas. This atmospheric pattern further supported the observed decrease in PM concentrations. However, following the cessation of rainfall, hotspot clusters reemerged between March 23 and 25, particularly in the southern zone of the Chiang Mai–Lamphun Basin. These clusters were concentrated in areas such as southern Chiang Mai, northern Tak, and the adjacent border regions of Myanmar. On March 23, 470 hotspots were recorded (accounting for 42% of the daily total), followed by 523 hotspots on March 24 (38%), and 634 on March 25 (31%).

Furthermore, the accumulated PERSIANN rainfall data from March 20–23, presented in Figure 6(k), reveals a widespread rain cluster across northern Thailand and Myanmar. This rainfall event, characteristic of summer storms, played a key role in removing $PM_{2.5}$ from the atmosphere through the process of wet deposition [54]. Rainfall significantly reduces the concentration of airborne pollutants, especially water-soluble particles such as sulfate, nitrate, and ammonium [55] and [56]. The removal efficiency depends on on factors including rainfall intensity and duration, the chemical composition of the rainwater, and prevailing meteorological conditions [48][57][58][59] and [60].

Additionally, the upper-level wind map from March 23 (Figure 6(l)) depicts airflow into northern Thailand originating from the west, southwest, and south, which aligns well with the HYSPLIT backward trajectory data for the same period. Multiple lines of scientific evidence support that northern Thailand and adjacent areas in neighboring countries lie within a shared "Transboundary Airshed". This means that air pollution can travel and disperse freely across political borders. In particular, the locations of hotspots within this region, combined with prevailing wind directions, play a significant role in influencing air pollution levels and fine particulate matter concentrations within the Chiang Mai–Lamphun urban area.

3.4 Vertical Structure and Dynamics of Air Pollution

Under typical atmospheric conditions, pollutant concentrations particularly particulate matter (PM) and other pollutants generally decrease with increasing altitude due to atmospheric processes and reduced influence from ground-level anthropogenic sources [61]. However, analysis of the vertical distribution and dynamics of air pollution using data from the DC-8 aircraft (Figure 8) revealed notable deviations from this pattern. Specifically, levoglucosan, a key tracer for open biomass burning (OBB), exhibited significant increases at specific altitude ranges. On March 18, elevated levels were detected between 1,500 and 2,000 meters in the morning and extended up to 3,000 meters in the afternoon. On March 25, pronounced concentrations were observed between 2,000 and 2,500 meters.

Furthermore, acetonitrile concentrations were observed to increase within specific altitude ranges across all four days. On March 16, afternoon measurements indicated higher values between 1,000–1,500 meters. On March 18, slight increases were noted during both morning and afternoon periods at altitudes ranging from 1,500 to 2,500 meters. A more pronounced increase was recorded on March 21 at altitudes between 1,500 and 2,000 meters. Lastly, on March 25, a modest elevation in concentration was detected in the morning within the 2,000 to 2,500 meter-altitude range. Regarding ozone, variations differed across the days, exhibiting both direct and inverse relationships with altitude. This distinction was particularly evident on March 18, where ozone levels showed a positive correlation with altitude during the morning, but an inverse correlation during the afternoon. In contrast, nitrogen dioxide (NO_2) consistently displayed an inverse correlation with altitude across all four days its concentration decreased as altitude increased.

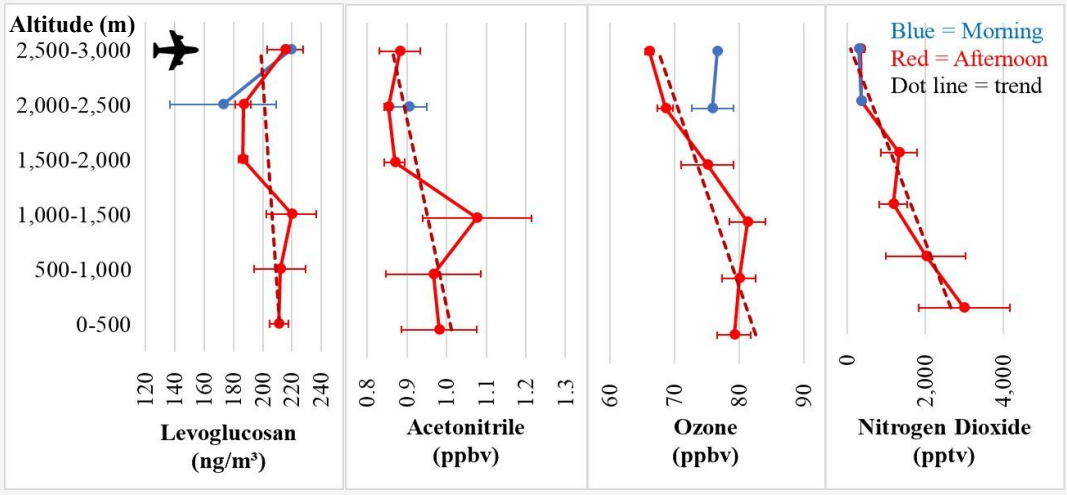

(a)

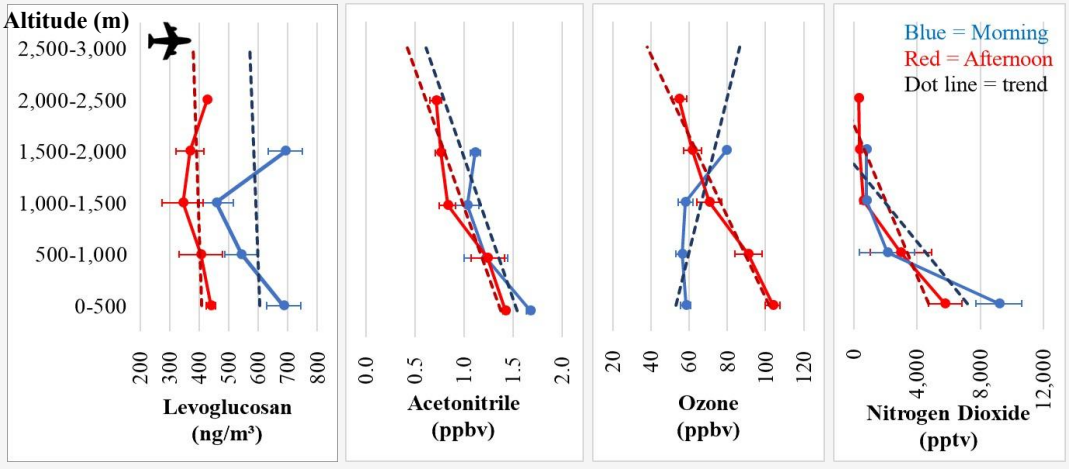

(b)

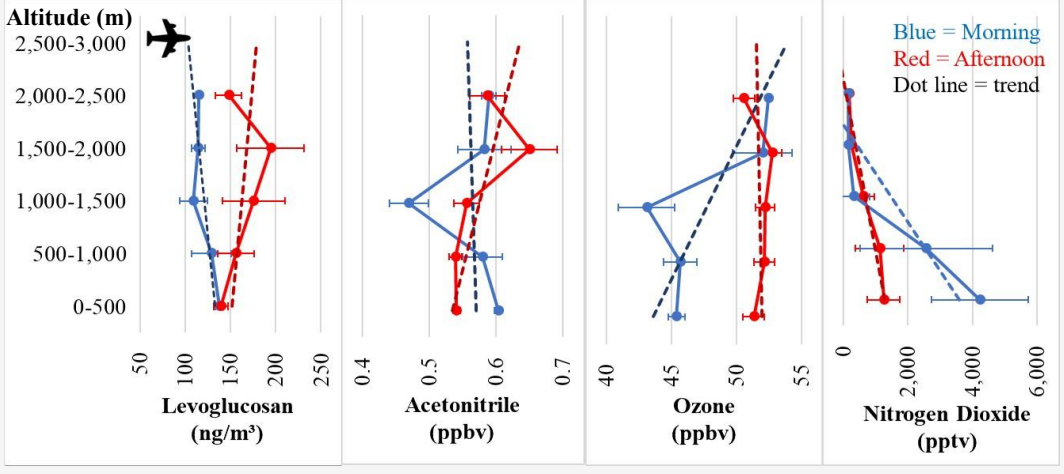

(c)

Figure 8: Air pollutant concentrations categorized by altitude levels (a) March 16 (b) March 18, (c) March 21, and (d) March 25, 2024 (continue next page)

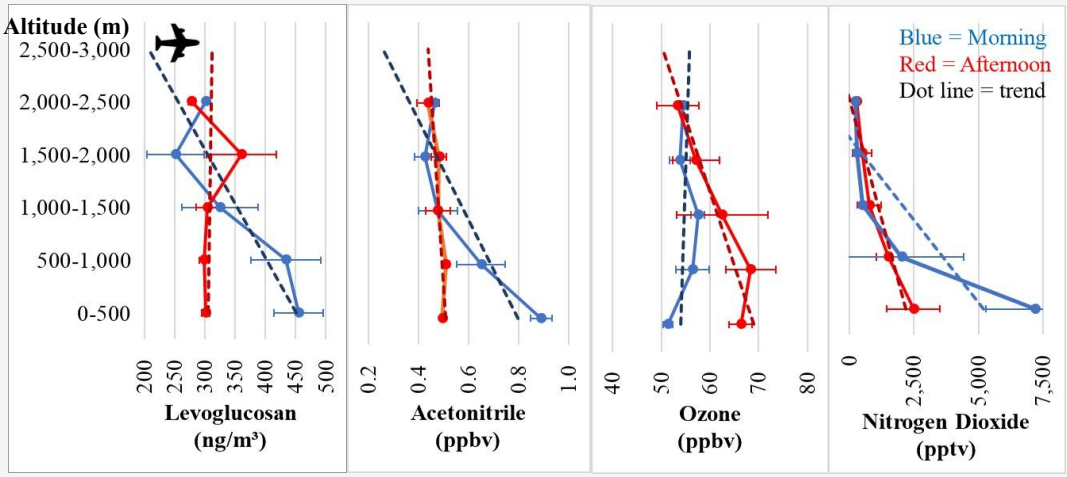

(d)

Figure 8: Air pollutant concentrations categorized by altitude levels (a) March 16 (b) March 18, (c) March 2, and (d) March 25, 2024 (continue from previous page)

3.5 Influence of Meteorological Factors on Air Pollution Dynamics

The analysis of upper-air meteorological data obtained from weather balloon soundings reveals critical factors contributing to the entrapment of air pollution near the surface in the Chiang Mai–Lamphun basin, as well as the causes of the accumulation of certain pollutants at varying altitudes. The results derived from the Skew-T Log-P diagrams on March 16, 18, 21, and 25, 2024 (Figure 9(a)–(d)) demonstrate clear changes in atmospheric stability structure, which directly affect the concentration of particulate matter in the study area. On March 16, 18, and 25, prominent temperature inversion layers were observed, accompanied by very low Convective Available Potential Energy (CAPE) values of 5.0, 0.0, and 3.0 Joules per kilogram, respectively. These values indicate a highly stable atmosphere with minimal convective activity, effectively acting as a "lid" that traps pollutants near the ground [62][63][64] and [65]. Conversely, on March 21, which coincided with rainfall, the Skew-T Log-P diagram indicated strong atmospheric uplift and a high CAPE value of 1,082.3 J/kg, reflecting an unstable atmosphere that promotes vertical mixing and dispersion of pollutants, thereby significantly reducing particulate matter concentrations.

Mechanistically, temperature inversion and low CAPE serve as key indicators of a stable atmosphere which suppresses vertical air movement, thereby facilitating the accumulation of air pollutants and particulate matter near the surface [62] and [63]. This phenomenon has been observed in regions such as the Eastern Alps, China, and arid climates like Kuwait [64], especially during winter when temperature inversions tend to be stronger and more persistent. Low CAPE values further confirm the atmosphere's inability to support buoyant vertical movement [65], maintaining stratified atmospheric layers and effectively inhibiting pollutant dispersion. Temperature inversion is a critical factor contributing to the trapping of air pollution within basin areas such as Chiang Mai–Lamphun [62][63][64] and [66]. Furthermore, this study found that air pollutants such as Levoglucosan tend to accumulate within atmospheric layers characterized by temperature inversions. Analysis of Skew-T Log-P diagrams on March 18 revealed the presence of multiple temperature inversion layers between approximately 3,000 and 4,000 meter-altitude. Combined with weak upper-level winds, these conditions restricted vertical pollutant dispersion, leading to the development of a vertical air recirculation zone [67], as depicted in the model presented in Figure 10.

Such recirculation zones play a crucial role in trapping particulate matter and pollutants both near the surface and within the lower atmospheric layers, thereby exacerbating haze conditions in Chiang Mai and Lamphun, despite no increase in pollution sources during that period. The thermodynamic structure of the atmosphere including inversion layers, wind patterns, and CAPE values exerts a direct influence on the transport, accumulation, and dispersion of pollutants within the lower troposphere [66][68] and [69].

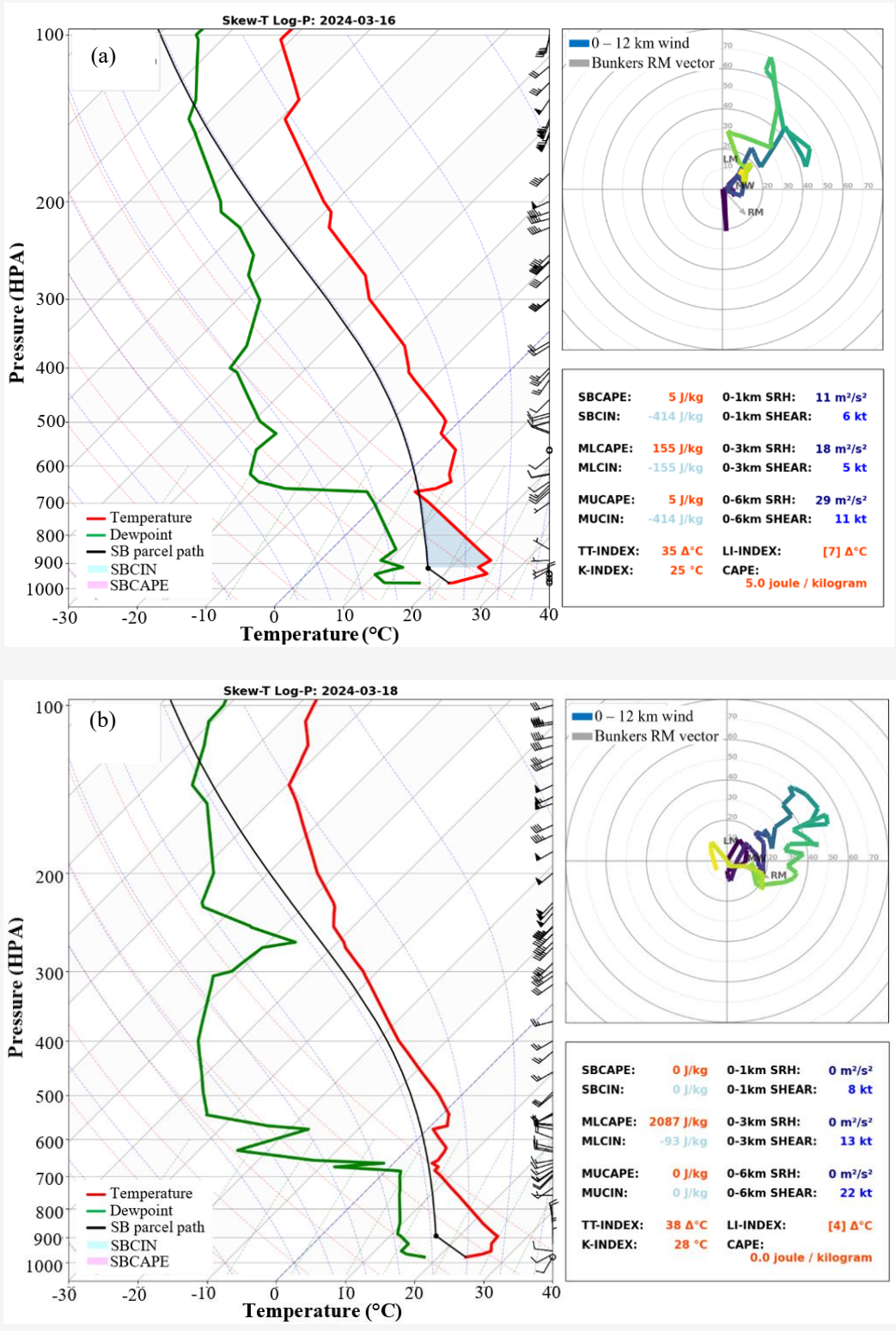

Figure 9: The Skew-T Log-P diagrams illustrate the vertical atmospheric profiles on March 16 (a), March 18 (b), March 21 (c), and March 25 (d) The red line represents temperature, the green line represents dew point, and the black dashed line indicates the parcel ascent (continue next page)

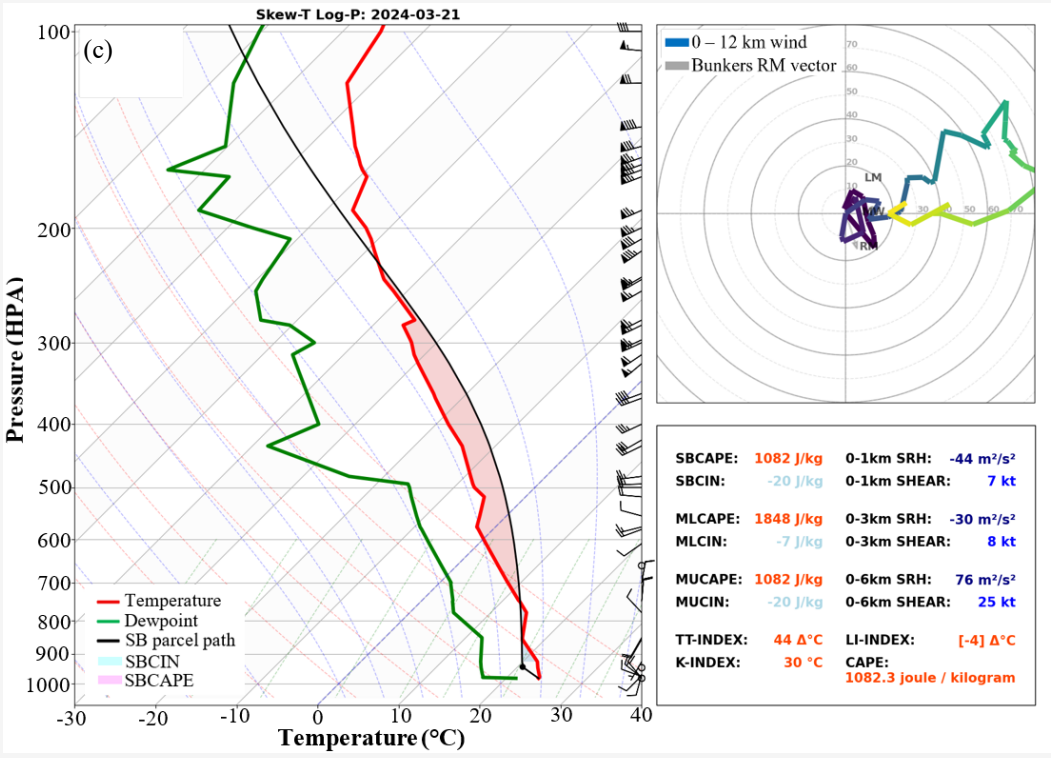

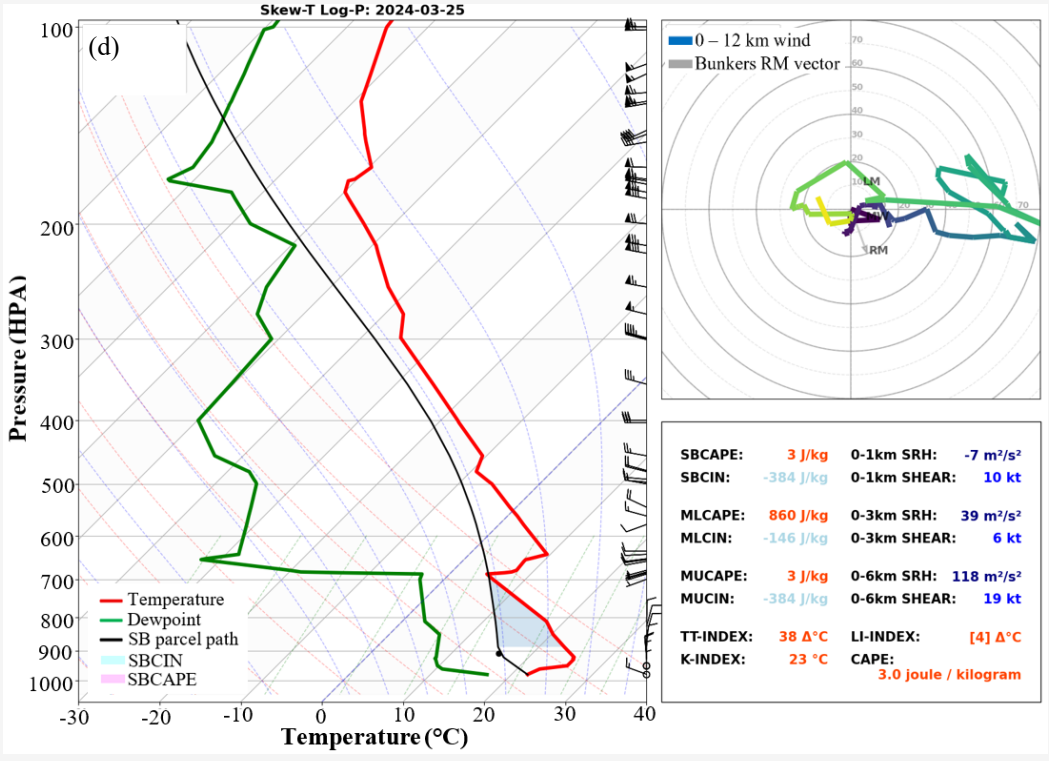

Figure 9: The Skew-T Log-P diagrams illustrate the vertical atmospheric profiles on March 16 (a), March 18 (b), March 21 (c), and March 25 (d) The red line represents temperature, the green line represents dew point, and the black dashed line indicates the parcel ascent (continue from previous page)

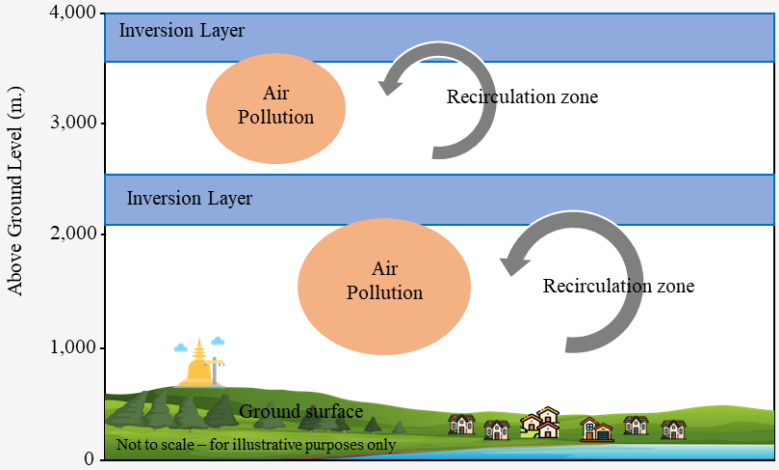

Figure 10: A vertical air pollution dynamics model in the Chiang Mai–Lamphun basin under temperature inversion conditions

In mountainous regions such as Sierra Nevada and Loški Potok (Slovenia), the vertical accumulation and dispersion of pollutants are influenced by local meteorological processes, including diurnal wind patterns and pronounced temperature fluctuations [66] and [70]. Surface-based inversions (SBI) and elevated inversions (EI) contribute to increased concentrations of aerosols, including $PM_{2.5}$ and black carbon, by limiting vertical air movement and trapping pollutants within the lower atmospheric layers [66].

Recirculation zones play a critical role in the processes of dust and aerosol retention by limiting the vertical dispersion and transport of pollutants. In urban environments, the interplay of complex local emission sources, meteorological conditions, and topographical features contributes to the development of recirculation zones, which in turn promote pollutant accumulation and hinder vertical air exchange [69]. A thorough understanding of these structural and dynamic processes is therefore crucial for formulating effective air pollution management strategies and designing efficient urban ventilation systems.

4. Conclusion

This study found that $PM_{2.5}$ concentrations were highest during the early morning hours and declined in the afternoon and evening, a pattern strongly linked to atmospheric stability and the presence of temperature inversion layers. Spatial analysis revealed that pollutant plumes exhibited temporal shifts in location, with significant accumulation observed in the western and southwestern parts of the study area. These patterns are consistent with hotspot data and results from the Backward Trajectory model, both of which suggest cross-border transport of air pollutants. Vertical atmospheric profiles obtained from NASA's DC-8 aircraft and radiosonde (sounding) data further illustrated the presence of multiple inversion layers and recirculation zones within the lower troposphere. These features significantly enhance pollutant accumulation, even in the absence of continuous local emissions.

In particular, the occurrence of persistent inversion layers between 1,500 and 4,000 meters above ground level, combined with weak upper-level winds, was found to be a key factor in trapping pollution both near the surface and at mid-atmospheric levels. The occurrence of recirculation further explains elevated concentrations of biomass burning markers such as levoglucosan in the mid-atmosphere, contributing to prolonged and severe haze episodes in the Chiang Mai–Lamphun basin, even during periods without ongoing combustion activities. The findings highlight the importance of incorporating vertical atmospheric dynamics into air pollution monitoring, rather than focusing solely on horizontal distributions. To improve the accuracy of air quality forecasts and the effectiveness of haze mitigation strategies particularly in topographically enclosed basins it is essential to integrate upper-air meteorological data, such as temperature inversion layers and upper-level wind patterns, into forecasting systems.

The insights gained from this study can support the development of real-time air quality early warning systems that incorporate atmospheric structural analysis alongside data from ground-based and airborne sensors. Additionally, the findings offer a scientific basis for the strategic design of pollution control zones, with a focus on regulating emissions along dominant wind pathways. Moreover, this approach facilitates more precise and seasonally adaptive emission reduction strategies by accounting for the prevailing patterns of air mass transport.

Although this study collected and analyzed data from multiple sources in detail, several limitations should be considered. Observations from the DC-8 aircraft were conducted only on select days March 16, 18, 21, and 25, 2024 leaving potential gaps in the temporal coverage of the air pollution episode. While HAZEMON sensor data were validated and adjusted against Pollution Control Department (PCD) station measurements, inaccuracies may still arise under high humidity or heavy rainfall conditions. Additionally, the meteorological data used in the HYSPLIT model has a spatial resolution of approximately 0.25 degrees, which may be insufficient to capture the finer-scale wind dynamics within the complex terrain of the Chiang Mai–Lamphun basin.

To strengthen the robustness of future analyses, it is recommended to implement more continuous monitoring of air pollution data both horizontally and vertically. The application of various technologies, such as radar systems or UAV-based sensors, could be utilized to mitigate limitations related to altitude data. Additionally, integrating data from cross-border areas should be considered to achieve a more accurate understanding of pollution transport originating from sources outside the study area. This study provides novel insights into the spatio-temporal dynamics of air pollution in Northern Thailand by integrating multiple observational platforms, including ground-based IoT sensors, reference PCD stations, NASA's DC-8 aircraft measurements, satellite products, meteorological datasets, and HYSPLIT trajectory modeling. The strength of this approach lies in the comprehensive integration of multi-source datasets, which enabled a simultaneous assessment of near-surface concentrations, vertical structures, and long-range transport mechanisms. Importantly, this study represents one of the early efforts to provide a detailed examination of temperature inversion layers in the Chiang Mai–Lamphun basin and their pivotal role in trapping pollutants during severe haze events. These findings emphasize the importance of incorporating both vertical and horizontal atmospheric information to accurately characterize air pollution dynamics in topographically complex basins.

In addition to advancing scientific understanding, the results demonstrate how integrated geospatial approaches can be effectively translated into practical applications. The spatial identification of $PM_{2.5}$ concentrations and their temporal fluctuations provides a foundation for developing real-time early-warning systems and targeted health advisories. Furthermore, the integration of VIIRS hotspot data with HYSPLIT backward trajectories enables the identification of both local and transboundary biomass burning sources, highlighting the urgent need for cross-border cooperation in haze mitigation. At the policy level, the findings emphasize the importance of enhancing government initiatives on air quality management, particularly through adaptive no-burn regulations during periods of high atmospheric pressure and in areas identified as high-risk by trajectory analysis. By bridging scientific innovation with actionable policy measures, this study offers both methodological advances and concrete pathways for policymakers and stakeholders to reduce $PM_{2.5}$ exposure and improve air quality in Northern Thailand.

Acknowledgments

The authors would like to express their sincere gratitude to Dr. James H. Crawford, Senior Research Scientist at NASA Langley Research Center, for his expert guidance and steadfast support throughout this study. Special thanks are also extended to Dr. Adisorn Lertsinsrubtavee, Director of intERLab at the Asian Institute of Technology (AIT), for his instrumental support in providing equipment, facilitating data access, and offering technical advice. Furthermore, the authors gratefully acknowledge the invaluable assistance from various institutions and their dedicated teams, including NASA, GISTDA, the Pollution Control Department (PCD) of Thailand, the Thai Meteorological Department (TMD), the ASIA-AQ Team, intERLab of AIT, and AiroTEC of Chiang Mai Rajabhat University (CMRU). Their contributions have significantly strengthened the quality and impact of this research.

References

[1] World Health Organization. *Ambient (Outdoor) Air Pollution*. [Online]. Available: https://www.who.int/news-room/fact-sheets/detail/ambient-(outdoor)-air-quality-and-health. [Accessed: Jun. 12, 2025].

[2] Thurston, G. and Lippmann, M., (2015). Ambient Particulate Matter Air Pollution and Cardiopulmonary Diseases. *Seminars in Respiratory and Critical Care Medicine*, Vol. 36(5), 934-942. https://doi.org/10.1055/s-0035-1549455.

[3] Health Effects Institute. *State of Global Air 2024: A Global Report on Air Quality and Health*. [Online]. Available: https://www.stateofglobalair.org. [Accessed: Jun. 12, 2025].

[4] State of Global Air. (2024). *Impact of Air Pollution on Life Expectancy*. [Online]. Available: https://www.stateofglobalair.org/health/life-expectancy. [Accessed: Jun. 17, 2025].

[5] Amnuaylojaroen, T., Kaewkanchanawong, P. and Panpeng, P., (2023). Distribution and Meteorological Control of PM2.5 and Its Effect on Visibility in Northern Thailand. *Atmosphere*, Vol. 14(3). https://doi.org/10.3390/atmos14030538.

[6] Inlaung, K., Chotamonsak, C., Macatangay, R. and Raksapatcharawong, M., (2024). Assessment of Transboundary PM2.5 from Biomass Burning in Northern Thailand using the WRF-Chem Model. *Toxics*, Vol. 12(7). https://doi.org/10.3390/toxics12070462.

[7] Supasri, T., Gheewala, S. H., Macatangay, R., Chakpor, A. and Sedpho, S., (2023). Association between Ambient Air Particulate Matter and Human Health Impacts in Northern Thailand. *Scientific Reports*, Vol. 13(1). https://doi.org/10.1038/s41598-023-39930-9.

[8] Parasin, N. and Amnuaylojaroen, T., (2024). Effect of PM2.5 on Burden of Mortality from Non-Communicable Diseases in Northern Thailand. *PeerJ*, Vol. 12. https://doi.org/10.7717/peerj.18055.

[9] Thongtip, S., Srivichai, P., Chaitiang, N. and Chanpheng, S., (2022). The Influence of Air Pollution on Disease and Related Health Problems in Northern Thailand. *Sains Malaysiana*, Vol. 51(7), 2075-2084. https://doi.org/10.17576/jsm-2022-5107-04.

[10] Jarernwong, K., Gheewala, S. H. and Sampattagul, S., (2023). Health Impact Related to Ambient Particulate Matter Exposure as a Spatial Health Risk Map Case Study in Chiang Mai, Thailand. *Atmosphere*, Vol. 14(2). https://doi.org/10.3390/atmos14020261.

[11] Sathitkunarat, S., Wongwises, P., Pan-Aram, R. and Chumkaew, P., (2008). Numerical Simulation of Terrain-Induced Mesoscale Circulation in the Chiang Mai Area, Thailand. *Meteorology and Atmospheric Physics*, Vol. 102(1), 113-121. https://doi.org/10.1007/s00703-008-0013-4.

[12] Chantara, S., (2012). *Air quality - Monitoring and Modeling: PM10 and Its Chemical Composition: A Case Study in Chiang Mai, Thailand. IntechOpen Journals*, 205-230. https://doi.org/10.5772/33086.

[13] Srivanit, M. and Hokao, K., (2012). Effects of Urban Development and Spatial Characteristics on Urban Thermal Environment in Chiang Mai Metropolitan, Thailand. *Lowland Technology International*, Vol. 14(2), 13-23.

[14] Ruttanawongchai, S., Raktham, C. and Khumsaeng, T., (2018). The Influence of Meteorology on Ambient PM2.5 and PM10 Concentration in Chiang Mai. *IOP Conference Series: Earth and Environmental Science*, Vol. 1144(1). https://doi.org/10.1088/1742-6596/1144/1/012088.

[15] IQAir. (2023). *World Air Quality Report 2023*. [Online]. Available: https://www.iqair.com/th/world-air-quality-report. [Accessed: Jun. 18, 2025].

[16] Li, W., Ge, P., Chen, M., Tang, J., Cao, M., Cui, Y., Hu, K., Nie, D. and Zhang, X., (2021). Tracers from Biomass Burning Emissions and Identification of Biomass Burning. *Atmosphere*, Vol. 12(11). https://doi.org/10.3390/atmos12111401.

[17] Araj, F. G., (2022). Saccharides as Particulate Matter Tracers of Biomass Burning: A Review. *International Journal of Environmental Research and Public Health*, Vol. 19(7). https://doi.org/10.3390/ijerph19074387.

[18] Caseiro, A. and Oliveira, C., (2012). Variations in Wood Burning Organic Marker Concentrations in the Atmospheres of Four European Cities. *Journal of Environmental Monitoring*, Vol. 14(7), 1872-1880. https://doi.org/10.1039/c2em10849f.

[19] Benetello, F., Squizzato, S., Hofer, A., Khan, B. M., Piazzalunga, A., Fermo, P., Formenton, M. G., Rampazzo, G. and Pavoni, B., (2017). Estimation of Local and External Contributions of Biomass Burning to PM2.5 in an Industrial Zone Included in a Large Urban Settlement. *Environmental Science and Pollution Research*, Vol. 24(8), 2100-2115. https://doi.org/10.1007/s11356-016-7987-0.

[20] Khan, Z. J., Sun, L., Tian, Y., Shi, G. and Feng, Y., (2021). Chemical Characterization and Source Apportionment of PM1 and PM2.5 in Tianjin, China: Impacts of Biomass Burning and Primary Biogenic Sources. *Journal of Environmental Sciences*, Vol. 101, 261-275. https://doi.org/10.1016/j.jes.2020.06.027.

[21] Zielinska, B. and Samburova, V., (2019). Residential and Non-Residential Biomass Combustion: Impacts on Air Quality. *Encyclopedia of environmental health*, Vol. 2, 499-507. https://doi.org/10.1016/B978-0-444-52272-6.00368-8.

[22] Shukri, S., Asmat, A., Rahiman, M., Japeiri, A., and Sahwee, Z. (2024). Real-time Vertical Air Quality Monitoring System Development for Urban Scale. *International Journal of Geoinformatics*, Vol. *20*(8); 102-114. https://doi.org/10.52939/ijg.v20i8.3463.

[23] Sharma, K. and Yadav, S., (2023). Air Quality Monitoring Using Geospatial Technology and Field Sensors. *Geospatial Analytics for Environmental Pollution Modeling*, 91-118. https://doi.org/10.1007/978-3-031-45300-7_4.

[24] Mishra, M., Sudarsan, D., Beja, S. K., Acharya, T., Santos, C. A. G., da Silva, R. M., Goswami, S. and Bhattacharyya, D., (2024). Air Quality Monitoring Using Geospatial Technology: A Bibliometric Analysis (1998–2021). *Air quality and human health*, 23-65. https://doi.org/10.1007/978-981-97-1363-9_3.

[25] NASA. (2022). *The Airborne and Satellite Investigation of Asian Air Quality (Asia-AQ): An Opportunity for International Collaboration*. [Online]. Available: https://espo.nasa.gov/missions/asia-aq. [Accessed: Jun. 12, 2025].

[26] Kanabkaew, T., Mekbungwan, P., Raksakietisak, S. and Kanchanasut, K., (2019). Detection of PM2.5 Plume Movement from IoT Ground Level Monitoring Data. *Environmental Pollution*, Vol. 252, 543-552. https://doi.org/10.1016/j.envpol.2019.05.082.

[27] Lertsinsrubtavee, A., Jayarathna, K. G. S., Mekbungwan, P., Kanabkaew, T. and Raksakietisak, S., (2022). Sea-Hazemon: Active Haze Monitoring and Forest Fire Detection Platform. *Proceedings of the 17th Asian Internet Engineering Conference (AINTEC '22)*, 88-95. https://doi.org/10.1145/3570748.3570761.

[28] Kanabkaew, T., Lertsinsrubtavee, A. and Raksakietisak, S., (2023). Detection of Forest Fires and Pollutant Plume Dispersion Using IoT Air Quality Sensors. *Environmental Pollution*, Vol. 338. https://doi.org/10.1016/j.envpol.2023.122701.

[29] Crawford, H. J., Travis, R. K., Judd, M. L., Lefer, L. B., Dibb, E. J., Kim, J., Park, R., Lee, G., Chang, L., Simpas, B. J., Cambaliza, O. M., Macatangay, C. R., Surapipith, V., Thongboonchoo, N., Thi Kim Oanh, N., Thi Hien, T., Thuy Ly, B., Salam, A., Ghude, S. D., Talib Latif, M., Yu, L. E., Tanimoto, H. and Kanaya, Y., (2022). The Airborne and Satellite Investigation of Asian Air Quality (Asia-AQ): An Opportunity for International Collaboration. *Proceedings of the IGARSS 2022-2022 IEEE International Geoscience and Remote Sensing Symposium*. IEEE. https://doi.org/10.1109/IGARSS46834.2022.9883819.

[30] Talbot, W. R. and Dibb, E. J., (2004). Aircraft-Based Measurements of Aerosols and Trace Gases. *Atmospheric Environment*, Vol. 38(12), 1731-1743.

[31] Schroeder, W., Oliva, P., Giglio, L. and Csiszar, I. A., (2014). The New VIIRS 375 m Active Fire Detection Data Product: Algorithm Description and Initial Assessment. *Remote Sensing of Environment*, Vol. 143, 85-96. https://doi.org/10.1016/j.rse.2013.12.008.

[32] NASA Earthdata. *VIIRS I-band 375 m Active Fire Data*. [Online]. Available: https://www.earthdata.nasa.gov/data/instruments/viirs/viirs-i-band-375-m-active-fire-data. [Accessed: Jun. 12, 2025].

[33] NASA. *Fire Information for Resource Management System (FIRMS)*. [Online]. Available: https://firms.modaps.eosdis.nasa.gov. [Accessed: Jun. 12, 2025].

[34] Takaku, J., Tadono, T., Doutsu, M., Ohgushi, F. and Kai, H., (2021). Updates of 'AW3D30 ALOS' Global Digital Surface Model in Antarctica with Other Open Access Datasets. *International Archives of the Photogrammetry, Remote Sensing and Spatial Information Sciences*, 401-408. https://doi.org/10.5194/isprs-archives-XLIII-B4-2021-401-2021.

[35] University of Wyoming. *Sounding Database*. [Online]. Available: http://weather.uwyo.edu/upperair/sounding.html. [Accessed: Jun. 17, 2025].

[36] Hsu, K. L. and Sorooshian, S., (2009). Hydrological Modelling and the Water Cycle: Coupling the Atmospheric and Hydrological Models: Satellite-Based Precipitation Measurement Using PERSIANN System. *Springer Nature*, 27-48. https://doi.org/10.1007/978-3-540-77843-1_2.

[37] Nguyen, P., Ashouri, H., Ombadi, M., Hayatbini, N., Hsu, K. and Sorooshian, S., (2020). PERSIANN-CDR for Hydrology and Hydro-Climatic Applications. *Satellite Precipitation Measurement*, 993-1012. https://doi.org/10.1007/978-3-030-35798-6_26

[38] Stein, F. A., Draxler, R. R., Rolph, D. G., Stunder, B. J. B., Cohen, D. M. and Ngan, F., (2015). NOAA's HYSPLIT Atmospheric Transport and Dispersion Modeling System. *Bulletin of the American Meteorological Society*, Vol. 96(12), 2059-2077. https://doi.org/10.1175/BAMS-D-14-00110.1.

[39] Draxler, R. R. and Hess, D. G., (1998). An Overview of the HYSPLIT_4 Modelling System for Trajectories, Dispersion, and Deposition (NOAA Technical Memorandum ERL ARL-224). *National Oceanic and Atmospheric Administration*, Air Resources Laboratory. [Online]. Available: https://www.arl.noaa.gov/wp_arl/wp-content/uploads/docu

ments/reports/arl-224.pdf. [Accessed: Jun. 17, 2025].

[40] Isaaks, E. H. and Srivastava, R. M., (1989). *An Introduction to Applied Geostatistics*. Oxford: Oxford University Press.

[41] Deng, L., (2015). Estimation of PM2.5 Spatial Distribution Based on Kriging Interpolation. *Proceedings of the International Conference on Intelligent Systems, Mechatronics and Manufacturing Engineering (ICISMME 2015)*, 1-5. https://doi.org/10.2991/ICISMME-15.2015.370.

[42] Xu, T., Liu, Y., Tang, L. and Zhang, Y., (2020). Improvement of Kriging Interpolation with Learning Kernel in Environmental Variables Study. *International Journal of Production Research*, Vol. 59(24), 7363-7378. https://doi.org/10.1080/00207543.2020.1856437.

[43] Thammaboribal, P., Tripathi, N.K., Ninsawat, S., and Pal, I. (2022). Earthquake Precursory Detection using Diurnal GPS-TEC and Kriging Interpolation Maps: 12 May 2008, Mw7.9 Wenchuan Case Study, *MethodsX*, Vol. 9; 101617, https://doi.org/10.1016/j.mex.2022.101617.

[44] Silverman, B. W., (1986). *Density Estimation for Statistics and Data Analysis*. London: Chapman and Hall.

[45] Ahlqvist, O., (2009). Overlay (in GIS). *International Encyclopedia of Human Geography*, Vol. 8, 48-55. https://doi.org/10.1016/B978-008044910-4.00487-9.

[46] Munoz, C. R., (2007). Morning Peak of Air Pollutant Concentrations in Urban Areas: Effect of Time Lag Between Emissions and Turbulence. *Atmospheric Environment*, Vol. 41(7), 1344-1359.

[47] Pu, B. and Moroni, E. A., (2023). Understanding Day–Night Differences in Dust Activities over the Dust Belt of North Africa, the Middle East, and Asia. *Atmospheric Chemistry and Physics Discussions*, Vol. 23(9), 5433-5466. https://doi.org/10.5194/acp-2022-490.

[48] Zhou, Y., Yue, Y., Bai, Y. and Zhang, L., (2020). Effects of Rainfall on PM2.5 and PM10 in the Middle Reaches of the Yangtze River. *Advances in Meteorology*, Vol. 2020. https://doi.org/10.1155/2020/2398146.

[49] Ramadhina, S. Q., (2023). Investigation of Rainfall Influence on Characteristics of Particulate Matter 2.5 in Jakarta City. *International Journal of Scientific Advances*, Vol. 4(6), 911-915.

[50] Dillayati, U. G., Wahyuni, D., Adriat, R., Azwar, A. and Zulfian, Z., (2024). Study on the Relationship between Hotspots and Air Pollution Standard Index Based on Carbon Monoxide Concentration in West Kalimantan. *Buletin Fisika*, Vol. 25(1), 81-88. https://doi.org/10.24843/bf.2024.v25.i01.p11.

[51] Khairullah, S. E. and Makmur, S. E. E., (2017). Trajectory and Concentration of PM10 on Forest and Vegetation Peat Fires: HYSPLIT Model Outputs and Observations. *IOP Conference Series: Earth and Environmental Science*, Vol. 58. https://doi.org/10.1088/1755-1315/58/1/012038.

[52] Wang, X., Chen, L., Guo, K. and Liu, B., (2022). Spatio-Temporal Trajectory Evolution and Cause Analysis of Air Pollution in Chengdu, China. *Journal of the Air & Waste Management Association*, Vol. 72(8), 876-894. https://doi.org/10.1080/10962247.2022.2058642.

[53] Ma, F., Gao, Q., Zhou, S., Su, F., Kang, N. and Sun, J., (2008). The Simulation and Analysis of a Typical Pollution Event around Beijing. *Research of Environmental Sciences*, Vol. 21(1), 30-36.

[54] Andronache, C., (2016). Dependence of Daily Aerosol Wet Deposition on Precipitation at Appalachian Mountains Site in the United States. *Aerosol and Air Quality Research*, Vol. 16(3), 665-673. https://doi.org/10.4209/aaqr.2015.05.0322.

[55] Xu, D., Ge, B., Wang, Z., Sun, Y., Chen, Y., Ji, D., Yang, T., Ma, Z., Cheng, N., Hao, J. and Yao, X., (2017). Below-Cloud Wet Scavenging of Soluble Inorganic Ions by Rain in Beijing during the Summer of 2014. *Environmental Pollution*, Vol. 230, 963-973. https://doi.org/10.1016/j.envpol.2017.07.033.

[56] Li, Y., Sun, J., Bi, Y., Wang, Q., Zhao, X., Lei, L., Du, A., Li, Z., Wang, Z., Pan, X., Han, C. and Sun, Y., (2023). New Insights into Scavenging Effect of Aerosol Species during Summer Rainfall Process in Beijing. *Journal of Geophysical Research: Atmospheres*, Vol. 128(15). https://doi.org/10.1029/2023JD038642.

[57] Han, L., Zhang, H.-L., Xiang, X., Zhang, P., Cheng, S. and Wei, W., (2017). Precipitation and Its Effects on Atmospheric Pollutants in a Representative Region of Beijing in Summer. *Environmental Science*, Vol. 38(6), 2211-2217.

[58] Speirs, N., Belden, J. and Hellum, A., (2023). The Capture of Airborne Particulates by Rain. *Journal of Fluid Mechanics*, Vol. 958, A40-1-A40-19. https://doi.org/10.1017/jfm.2023.101.

[59] Zhao, X., Sun, Y., Zhao, C. and Jiang, H., (2020). Impact of Precipitation with Different Intensity on PM2.5 over Typical Regions of China. *Atmosphere*, Vol. 11(9). https://doi.org/10.3390/atmos11090906.

[60] Ou, S., Wei, W., Cai, B., Chen, S., Guan, P. and Cheng, S., (2022). The Independent Impacts of PM2.5 Dropping on the Physical and Chemical Properties of Atmosphere over North China Plain in Summer during 2015-2019. *Sustainability*, Vol. 14(7). https://doi.org/10.3390/su14073930.

[61] Yin, Z., Yuan, L., Yang, Y., Wu, X., Chen, Z. and Long, H., (2025). Exploring the Altitude Differentiation and Influencing Factors of PM2.5 and O3: A Case Study of the Fenwei Plain, China. *Frontiers in Environmental Science*, Vol. 12. https://doi.org/10.3389/fenvs.2024.1509460.

[62] Piringer, M. and Baumann-Stanzer, K., (2024). The Role of Temperature Inversions in Air Pollution Episodes Demonstrated by Examples in the Eastern Alps (Austria). [Online]. Available: https://oxfordre.com/climatescience/display/10.1093/acrefore/9780190228620.001.0001/acrefore-9780190228620-e-944. [Accessed: Jun. 17, 2025].

[63] Huang, Q., Chu, Y. and Li, Q., (2021). Climatology of Low-Level Temperature Inversions over China Based on High-Resolution Radiosonde Measurements. *Theoretical and Applied Climatology*, Vol. 144(1), 415-429. https://doi.org/10.1007/s00704-021-03536-w.

[64] Al-Hemoud, A., Al-Sudairawi, M., Al-Rashidi, M. S., Behbehani, W. and Al-Khayat, A., (2019). Temperature Inversion and Mixing Height: Critical Indicators for Air Pollution in Hot Arid Climate. *Natural Hazards*, Vol. 97(1), 139-155. https://doi.org/10.1007/s11069-019-03631-2.

[65] Parker, D. J., (2002). The Response of CAPE and CIN to Tropospheric Thermal Variations. *Quarterly Journal of the Royal Meteorological Society*, Vol. 128(581), 119-136. https://doi.org/10.1256/00359000260498815.

[66] Glojek, K., Mocnik, G., C-Alas, D. H., Cuesta-Mosquera, A., Drinovec L., Gregoric, A., Ogrin, M., Weinhold, K., Jezek, I., Muller, T., Rigler, M., Remskar, M., van-Pinxteren, D., Herrmann, H., Ristorini, M., Merkel, M., Markelj, M, and Wiedensohler, A., (2020). The Impact of Temperature Inversions on Black Carbon and Particle Mass Concentrations from Wood-Burning in a Mountainous Area. *EGUsphere*, *EGU2020-21310.* https://doi.org/10.5194/egusphere-egu2020-21310.

[67] Naizabayeva, L., Zaitov, D. and Seilova, N., (2024). Integrating Smart Traffic Systems with Real-Time Air Quality Monitoring to Minimize Emissions and Improve Urban Health. *Procedia Computer Science*, Vol. 251, 603-608. https://doi.org/10.1016/j.procs.2024.11.156.

[68] Li, H., Liu, B., Ma, X., Ma, Y., Jin, S., Fan, R., Wang, W., Fang, J., Zhao, Y. and Gong, W., (2022). The Influence of Temperature Inversion on the Vertical Distribution of Aerosols. *Remote Sensing*, Vol. 14(18). https://doi.org/10.3390/rs14184428.

[69] Salmond, J. A. and McKendry, I. G., (2009). Chapter 2: Influences of Meteorology on Air Pollution Concentrations and Processes in Urban Areas. *Air quality in urban environments*, Vol. 28, 23-41. https://doi.org/10.1039/9781847559654-00023.

[70] Jaen, C., Titos, G., Castillo, S., Casans, A., Rejano, F., Cazorla, A., Herrero, J., Alados-Arboledas, L., Grimalt, J. O. and van Drooge, B. L., (2023). Diurnal Source Apportionment of Organic and Inorganic Atmospheric Particulate Matter at a High-Altitude Mountain Site under Summer Conditions (Sierra Nevada; Spain). *Science of the Total Environment*, Vol. 905, 167178. https://doi.org/10.1016/j.scitotenv.2023.167178.